

Validation and development of wall-function models for Liquid Rocket Engine applications

*G. Indelicato**, *A. Remiddi**, *P. E. Lapenna** and *F. Creta**

** Sapienza University of Rome*

via Eudossiana 18 - 00184 Rome, Italy

Corresponding author: giuseppe.indelicato@uniroma1.it

Abstract

In this work algebraic wall-function models for the prediction of thermo-mechanical loads in rocket-engine applications are explored and investigated. To this end two categories of turbulent wall-bounded flows are identified: a non-premixed flame impinging parallel to an isothermal wall and a cryogenic stream flowing in a heated pipe at high pressure. For the mentioned configurations, reference solutions are used for the sake of validation from experimental and numerical campaigns. For the former configuration, wall-function models from literature are first categorized based on the degree of modelling of the thermal field and then applied to the simulation of a realistic single-injector oxygen/methane rocket chamber. For the latter, an extension of one of the model selected from the previous analysis is proposed in order to deal with real-gas conditions. Results show that while wall-heat-flux predictions are well reproduced by the proposed wall-modeled framework and by algebraic wall-functions as long as the kinematic-thermal coupling is retained, applications of algebraic wall-functions to cryogenic high pressure flows still require further advancements in order to provide reliable predictions of key wall quantities.

1. Introduction

Nowadays high pressure turbulent combustion is a topic of interest for a number of applications, from industrial burner up to diesel and rocket engines. In this context the numerical investigation of high pressure, turbulent and reactive flows by means of Computational Fluid Dynamics (CFD) is an attractive tool both for the design of realistic combustion chambers and both from a more fundamental perspective, such as the analysis of mixing dynamics and flame structures at high pressure.

Progressively more reliable and affordable multi-dimensional simulations are to these days performed, especially prompted by the development of High Performance Computing (HPC) algorithms and infrastructures. However, the realization of such complex simulations is still associated to numerical challenges far from being solved. Among the many, one is the computational bottleneck associated to boundary layer resolution of high-Reynolds number flows, such as those found in Liquid Rocket Engine (LRE) applications.

These kind of flows are generally characterized by extreme thermodynamic conditions and substantial variation of properties during nominal operative conditions. In this context an example is given by propellant injection, which generally occurs at high pressure and cryogenic temperatures and is then followed by mixing and combustion processes, or by the regenerative cooling system of a LRE, where the fluid enters the system under cryogenic conditions and is then heated up by the heat flux from the combustion chamber. The mentioned situations induce substantial variation of properties in the near-wall field which makes the numerical modeling of such flows even more complex.

In this context wall-modeled simulations are conceived in order not to solve the turbulent boundary layer down to the wall and save computational resources. However huge modeling efforts of the wall and of the near-wall field are required. Wall functions in particular are generally employed to provide algebraic expressions for wall shear stress and wall heat flux as boundary conditions of the flow.

In this context the objective of the present work is to validate a wall-modeled framework in an Unsteady Reynolds Averaged Navier Stokes (uRANS) context and propose wall-function models for LRE applications under stratified conditions. To this end, wall-modeled analysis from 2D and 3D uRANS and Large Eddy Simulations (LES) are presented. For the former the configuration taken as reference is an experimental gaseous oxygen/methane (GOx/GCH₄) single-injector combustor developed at TUM; while for the latter a database of wall-resolved LES (WR-LES) of cryogenic poara-hydrogen in a heated pipe is presented with the final aim of proposing an algebraic wall function model amenable to any arbitrary Equation of State (EoS). Following this rationale, the work is organized as follow: Section

VALIDATION AND DEVELOPMENT OF WALL-FUNCTIONS FOR LRE

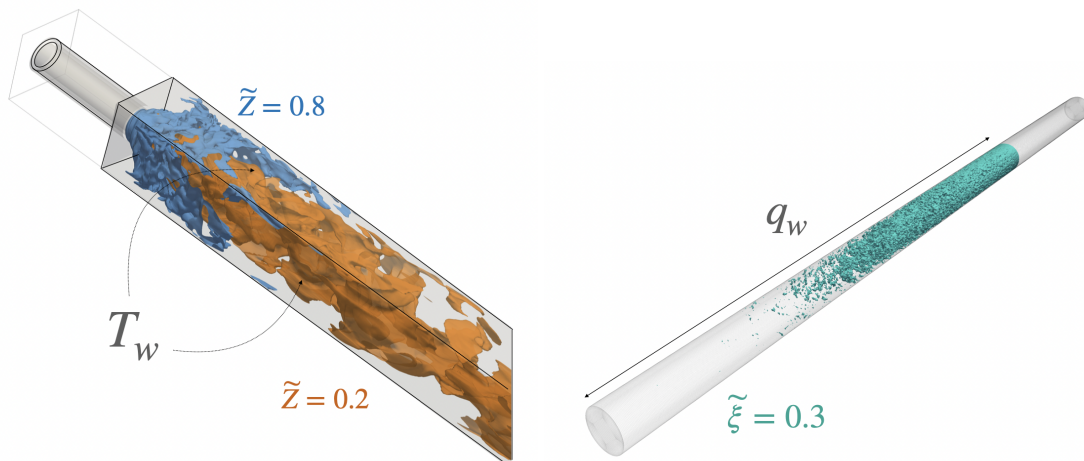


Figure 1: Schematic representation of the configurations object of this study.

I provides a description of the numerical and experimental configurations employed as reference for the present work; Section II gives a description of the numerical framework used to generate the presented simulations; Section III reports details of the proposed wall-modeled framework and the wall-functions employed; finally in Section IV results of the applications are shown. Summary and conclusions of the work are finally reported.

2. Investigated configurations

The configurations investigated in the present work envisage:

1. a turbulent non-premixed flame parallel to an isothermal wall
2. a cryogenic high-pressure flow through an heated pipe

The mentioned configurations are depicted in Fig. 1 and in common LRE are representative of the turbulent wall heat transfer process between the reactive mixture and the combustion chamber walls and of the heating of the propellant stream in the regenerative cooling channels of a LRE due to the heat coming from the combustion chamber, respectively. Indeed the latter configuration can also be found inside the propellant inlets, where a thermal break-up mechanism has been recently observed to play an important role in the injection of a LRE under high-pressure, cryogenic conditions.

2.1 Experimental single-injector GO_x/GCH₄ combustor

The experimental facility developed at the Technical University of Munich is taken as reference for the first case-study. It is a single-element GCH₄/GO_x combustor²¹ capacitively cooled for which experimental data are provided in terms of axial pressure, temperature on the and reconstructed wall heat flux.²³ The chamber has a square cross section of 12 mm × 12 mm. Propellants are injected through a coaxial injector at the operating conditions of $p = 20$ bar, $T_{Ox} = 278$ K and $T_F = 269$ K and at an Oxidizer to Fuel Ratio (ROF) of 2.6. The mass flow rates of oxidizer and fuel are 0.0045 kg/s and 0.0017 kg/s, respectively and the computational domain is truncated at the nozzle inlet due to the low-Mach number numerical framework described in the next section. The injector channels are not simulated and turbulent conditions are imposed in inlet based on standard RANS approach. Adiabatic conditions are imposed on the post-tip and on the plate wall while a temperature profile extracted from experiments is applied all over the upper chamber wall as isothermal boundary condition.

2.2 Numerical pipe flow in supercritical and cryogenic conditions

As a second case-study, a numerical configuration is proposed and investigated by the authors. It is a cylindrical pipe of diameter $D = 0.16$ mm and length $L = 50D$, with a first unheated $15D$ segment to let turbulence develop and the remaining $35D$ with a constant wall heat flux imposed to heat the flow. A zero-gradient boundary condition is applied on the pipe outlet section for velocity, while in inlet a Dirichlet condition equal to 18.4016 m/s is imposed, resulting in

Run	q_w (MW/m ²)	$T_{b,max}$ (K)	$Re_{b,max}$ (-)
SP-Q1	1	30	21000
SP-Q2	2	41	33000
SP-Q3	3	53	48000
SP-Q5	5	73	52000

Table 1: Key quantities of the WR-LES database for the cryogenic pipe configuration of Fig. 1. The subscript b refers to bulk quantities while maximum values are attained on the outlet section. $Re_b = (\rho U)_b D / \mu_b$.

a Reynolds number of 16000 based on this value, on the pipe diameter and on the inlet viscosity $\mu = \mu(T_{in} = 25 \text{ K}; p_0)$. Pressure is fixed on the outlet section at $p_0 = 5 \text{ MPa}$ while in inlet is given by a Neumann boundary condition. Turbulent conditions are prescribed in inlet based on a vortex method with a decaying turbulence inflow generator.¹³ Based on that a plug flow velocity profile is imposed as target profile and perturbations are superimposed based on prescribed values of the Reynolds stress tensor components. The latter are estimated assuming a turbulence intensity of 10% with respect to the bulk inlet velocity.

Different values of wall heat flux q_w are parametrically imposed on the mentioned configuration. The aim is to progressively heat-up the fluid (cryogenic para-hydrogen) and see the pseudo-boiling transition inside the pipe. An error function is imposed between the unheated and heated segments in order to have a continuous wall boundary condition. Tab. 1 briefly reports a summary of each case of the database.

3. Numerical framework

All the simulations presented in this contribution are obtained within the OpenFOAM³⁰ C++, open-source platform and the OpenSMOKE++⁶ library. In particular the solver *flameletSMOKE* developed by the CRECK modeling group has been selected as reference and in-house modified to deal with rocket-relevant applications. The choice of the mentioned solver is motivated by the flamelet tabulated approach²⁴ on which the thermo-physical model of the flow is based. In particular the native non-adiabatic version of the flamelet look-up tables calculation,¹⁶ originally intended for radiation problems, has been extended to deal with non-adiabatic losses inside a LRE combustion chamber as described in Indelicato et al.¹⁰

In the low-Mach number formulation of the governing equations it can be shown that the mentioned tabulated approach is easily extendable to single-species¹⁴ flows as long as the mixture fraction Z , on which the thermo-chemistry of a reactive mixture is mapped according to the standard flamelet theory,²⁴ is replaced by a non-dimensional temperature denoted in the following as ξ and defined as $\xi = (T - T_{min}) / (T_{max} - T_{min})$, where T is temperature. This allows to pre-compute thermodynamic and transport properties of the flow (para-hydrogen for the single-species configuration of Section 2) and store them in a looked-up table interpolated at run-time based on entry values of ξ , being $\bar{\cdot}$ the Favre-averaged operator. The temperature extremes T_{max} and T_{min} are selected in order to enclose the maximum and minimum temperature expected in the simulated field. In the present work they are set to 20 and 1000 K respectively. The mentioned solver is based on a pressure-based approach and employs the Pressure Implicit with Splitting of Operators (PISO) segregated algorithm to solve the governing equations. The latter are written in the low-Mach number limit and are briefly summarized below for a reactive mixture assuming unitary and constants Lewis numbers:

$$\frac{\partial \bar{p}}{\partial t} + \nabla \cdot (\bar{\rho} A_D^{-1} H) = \nabla \cdot (\bar{\rho} A_D^{-1} \nabla \bar{p}) \quad (1)$$

$$\frac{\partial (\bar{\rho} \bar{U})}{\partial t} + \nabla \cdot (\bar{\rho} \bar{U} \bar{U}) = -\nabla \bar{p} + \nabla \cdot \bar{\tau} \quad (2)$$

$$\frac{\partial (\bar{\rho} \bar{Z})}{\partial t} + \nabla \cdot (\bar{\rho} \bar{U} \bar{Z}) = \nabla \cdot \left[\left(\bar{\alpha} + \frac{\mu_t}{S c_t} \right) \nabla \bar{Z} \right] \quad (3)$$

$$\frac{\partial (\bar{\rho} \bar{Z}''^2)}{\partial t} + \nabla \cdot (\bar{\rho} \bar{U} \bar{Z}''^2) = \nabla \cdot \left[\left(\bar{\alpha} + \frac{\mu_t}{S c_t} \right) \nabla \bar{Z}''^2 \right] + C_g \left(\bar{\alpha} + \frac{\mu_t}{S c_t} \right) |\nabla \bar{Z}|^2 - C_d \bar{\rho} \frac{\epsilon}{k} \cdot \bar{Z}''^2 \quad (4)$$

$$\frac{\partial (\bar{\rho} \bar{h})}{\partial t} + \nabla \cdot (\bar{\rho} \bar{U} \bar{h}) = \nabla \cdot \left[(\bar{\alpha} + \alpha_t) \nabla \bar{h} \right] \quad (5)$$

In Eqs. (1)-(5) t is time, ρ is density, A_D and H matrices coming from the discretization of momentum equation in a finite-volume context,^{7,18} p is pressure, $\bar{\tau}$ the stress tensor given by $\bar{\tau} = \mu_{eff} (\nabla \bar{U} + \nabla \bar{U}^T - 2/3 (\nabla \cdot \bar{U}) \bar{I})$, where μ_{eff}

VALIDATION AND DEVELOPMENT OF WALL-FUNCTIONS FOR LRE

denotes an effective viscosity consisting of a laminar μ and turbulent μ_t contributions; The latter is modeled as $\rho C_\mu \frac{k^2}{\epsilon}$ in a uRANS context, with ϵ and k the turbulent energy dissipation and production, respectively, coming from the $k - \epsilon$ turbulence model, and C_μ a model constant equal to 0.09; in LES μ_t is given by the WALE closure model;²⁰ U is the velocity vector, Z the mixture fraction, α the thermal diffusivity (kg/ms) and Sc_t a turbulent Schmidt number. C_g and C_d are default model constants equal to 2.86 and 2.

For the single-species flow configuration, the transport equation for the specific static enthalpy h (Eq. (5)) is replaced by a transport equation in ξ :

$$\frac{\partial(\bar{\rho}\tilde{\xi})}{\partial t} + \nabla \cdot (\bar{\rho}\tilde{U}\tilde{\xi}) = \frac{1}{c_p} \nabla \cdot [(\tilde{\lambda} + \lambda_t) \nabla \tilde{\xi}] \quad (6)$$

where c_p is the specific heat while λ the laminar thermal conductivity of the flow; λ_t is modeled as $\lambda_t = c_p \alpha_t$. Equations (3) and (4) are not solved. Transport equations for the turbulent kinetic energy k and dissipation ϵ from the $k - \epsilon$ model are also reported:

$$\frac{\partial(\bar{\rho}k)}{\partial t} + \nabla \cdot (\bar{\rho}\tilde{U}k) = \nabla \cdot \left[\left(\bar{\mu} + \frac{\bar{\rho}v_t}{\sigma_k} \right) \nabla k \right] + \bar{\rho}P_k - \frac{2}{3}\bar{\rho}\nabla \cdot Uk - \bar{\rho}\epsilon \quad (7)$$

$$\frac{\partial(\bar{\rho}\epsilon)}{\partial t} + \nabla \cdot (\bar{\rho}\tilde{U}\epsilon) = \nabla \cdot \left[\left(\bar{\mu} + \frac{\bar{\rho}v_t}{\sigma_\epsilon} \right) \nabla \epsilon \right] + C_1 \bar{\rho}P_k \frac{\epsilon}{k} - \frac{2}{3}(C_1 - C_3)\bar{\rho}\nabla \cdot U\epsilon - C_2 \bar{\rho} \frac{\epsilon^2}{k}. \quad (8)$$

In Eqs. (7)-(8) P_k is the turbulence production term, while σ_k , σ_ϵ , C_1 , C_2 and C_3 are default model constants. All the thermo- and transport properties required by the governing equations (1)-(6), such as density, specific heat or viscosity, are interpolated at run-time from looked-up tables accessed by specific entry values. In particular for the simulation of reactive mixtures the generic extracted property $\tilde{\psi}$ is given as $\tilde{\psi}(\tilde{Z}, \tilde{Z}''^2, \tilde{\chi}_{st}, \tilde{\phi}; p_0)$ said ϕ an enthalpy defect calculated at run-time as:

$$\tilde{\phi} = \frac{\tilde{h} - \tilde{h}_{ad}(\tilde{Z})}{f(\tilde{Z})} \quad (9)$$

and measuring deviations from adiabatic conditions $\tilde{h}_{ad}(\tilde{Z})$ based on the function $f(\tilde{Z})$ modulating the enthalpy loss in the mixture fraction space;^{10,12} p_0 is the background thermodynamic pressure at which properties are computed; χ_{st} is the scalar dissipation rate conditioned to the stoichiometric mixture fraction value, which is retrieved from the mean scalar dissipation rate $\tilde{\chi}$. The latter is modeled as $C_\chi \frac{\epsilon}{k} \tilde{Z}''^2$ in uRANS.

For the single-species flow configuration tabulated properties read $\tilde{\psi} = \tilde{\psi}(\tilde{\xi}; p_0)$, with $\tilde{\xi}$ given by the solution of its transport equation (6). Figure 2 schematically displays the look-up process and tables structure associated to each configuration.

4. Wall-modeling

Main scope of the present work is to validate and propose wall-modelling strategies for LRE applications based on wall-function models. Among numerical and algebraic models, based on the categorization proposed in,^{4,5} only the latter will be explored here, serving as approximate wall-boundary conditions for turbulent quantities appearing in the governing equations (1)-(6). Specifically, wall-function models are needed to prescribe wall-values for v_t ($v_{t,w}$) and α_t ($\alpha_{t,w}$) and near-wall values of ϵ and P_k (ϵ_P and $P_{k,P}$, the subscript P denoting the location of the wall-adjacent node). Since we are mostly interested in wall-heat-transfer predictions, our aim is to explore different wall-functions for $\alpha_{t,w}$ while keeping fixed the ones for $v_{t,w}$, ϵ_P and $P_{k,P}$ which read:

$$v_{t,w} = v_w \left(\frac{\kappa y^+}{\ln(Ey^+)} - 1 \right) \quad (10)$$

$$\epsilon_P = \left(\frac{\rho_w}{\rho_P} \right)^{3/2} \frac{u_\tau^3}{\kappa \Delta y} \quad (11)$$

$$P_{k,P} = (v_w + v_{t,w}) \left(\frac{\rho_w}{\rho_P} \right)^{3/2} \frac{d\tilde{U}_P}{dy} \frac{u_\tau}{\kappa \Delta y} \quad (12)$$

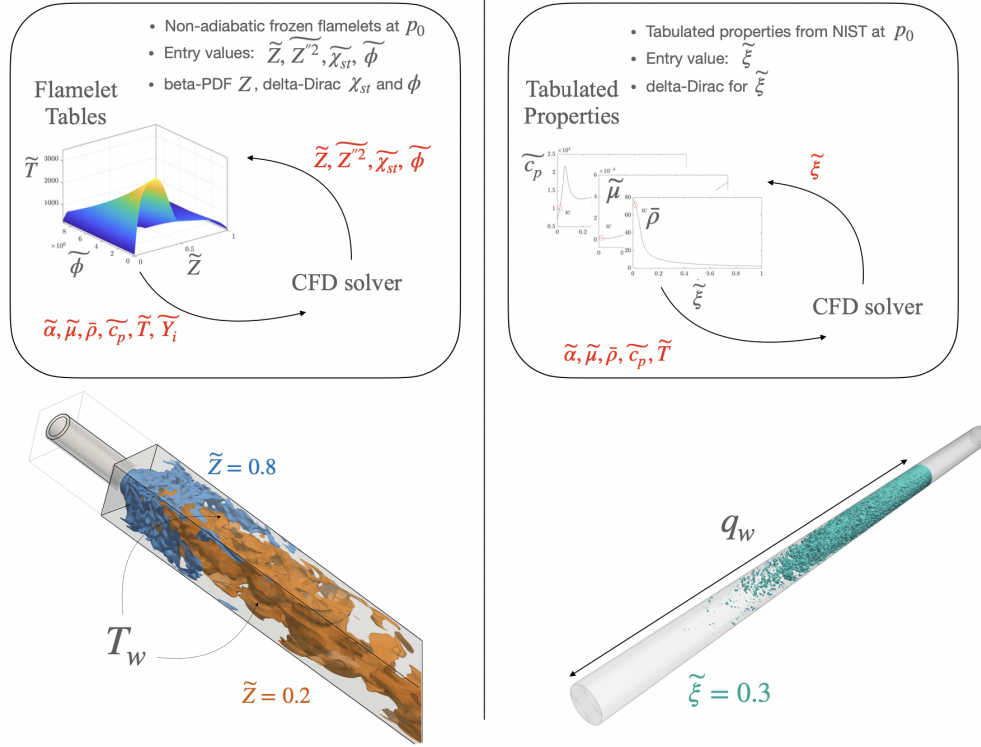


Figure 2: Schematic view of the look-up process and summary of tabulated properties for each investigated configuration.

In the above equations $\kappa = 0.41$ is the von Karman constant, $E = 9.8$, $y^+ = u_\tau \Delta y / \nu_w$ is the non-dimensional wall distance with Δy the distance of the first computational node from the wall and u_τ the skin friction velocity; in a RANS and uRANS context the latter is given by the following turbulence closure for stratified flows:¹⁰

$$u_\tau = \left(\frac{\rho_p}{\rho_w} \right)^{1/2} C_\mu^{1/4} \sqrt{k_p} \quad (13)$$

4.1 Wall-function models for $\alpha_{t,w}$

In order to close the system of governing equations and respective boundary conditions, we need to determine a model for $\alpha_{t,w}$. Although regarding turbulent combustion problems a wide literature on algebraic wall-functions for wall-heat-flux predictions in Internal Combustion (IC) engines^{2,9,25,26} exists and more recently selected models were proposed for rocket engines,^{3,19} for cryogenic high pressure flows no dedicated models exist to the best of authors' knowledge. Therefore, referring to the case studies individuated in Section 2, wall-functions from both the IC and the rocket engine literature have been selected, categorized, adapted and finally applied to uRANS simulations of LRE combustion chambers; Specifically three categories of wall-functions for $\alpha_{t,w}$ are defined:

- *Reynolds analogy* (RA-WF): assuming the kinematic and thermal boundary layers to be similar and the near-wall thermal field to be isotropic, it is possible to define a turbulent thermal diffusivity on the wall by scaling the turbulent viscosity with a constant turbulent Prandtl number Pr_t :

$$\alpha_{t,w} = \frac{\bar{\rho}_w \nu_{t,w}}{Pr_t} \quad (14)$$

that is, $\alpha_{t,w}$ only depends on the chosen law for the wall turbulent viscosity which in the present work is given by Eq. (10).

- *Thermal wall-function* (TH-WF): a category of wall functions obtained from the integration of the energy equation in the boundary layer generally assuming:^{1,9}

VALIDATION AND DEVELOPMENT OF WALL-FUNCTIONS FOR LRE

- (a) wall normal gradients greater than those parallel to the wall
- (b) negligible pressure gradients
- (c) no Dufour or Soret effects nor radiation phenomena
- (d) ideal gas assumption

In particular the model chosen in the present work is the one developed by Han and Reitz⁹ for IC engines, according to which for a given isothermal condition T_w imposed on the wall, the modeled wall-heat-flux is given under frozen chemistry condition as:

$$q_w = \frac{u_\tau(\rho c_p T)_P \ln(T_P/T_w)}{2.1 \ln(y^+) + 2.5} \quad (15)$$

The turbulent thermal diffusivity at the wall is then obtained as:

$$\alpha_{t,w} = \frac{q_w}{c_{p,w} \frac{\partial T}{\partial y}} - \bar{\alpha}_w \quad (16)$$

which comes from the Fourier law for the heat flux in a wall-modeled context.

- *Coupled wall-function (C-WF)*: in this class of models the mutual interaction between velocity and temperature in the near-wall region is retained in the derivation. Examples are the models of Nichols et al.¹⁹ and Cabrit and Nicoud.³ The latter is in particular employed in the present work and its main derivation steps are briefly outlined below:

- 1) first an analytical law relating temperature T to velocity U in the near-wall region is defined:

$$\frac{T}{T_w} = D - B_q Pr_t U^+ \quad (17)$$

being D an integration constant depending on the Prandtl number of the fluid on the wall, $B_q = T_\tau/T_w$ the heat transfer coefficient, $U^+ = U/u_\tau$ and T_τ the friction temperature;

- 2) then the van Driest's compressible velocity transformation²⁹ is assumed valid:

$$\int_0^{U^+} \left(\frac{\rho}{\rho_w} \right)^{1/2} dU^+ \approx \frac{1}{\kappa} \ln(y^+) + C \quad (18)$$

with $C = 5.5$

- 3) substituting $\rho/\rho_w = T_w/T$ (assuming $R = R_w$ with R the gas constant and pressure imposed from the outer flow, $p = p_w$) inside Eq. (18) leads to:

$$\int_0^{U^+} \left(\frac{T_w}{T} \right)^{1/2} dU^+ \approx \frac{1}{\kappa} \ln(y^+) + C \quad (19)$$

which can be solved analytically to give:

$$\frac{2T_w}{Pr_t T_\tau} \left(\sqrt{D} - \sqrt{\frac{T_P}{T_w}} \right) \approx \frac{1}{\kappa} \ln(y^+) + C \quad (20)$$

The friction temperature T_τ appearing inside Eq. (20) is then expressed as a function of u_τ by recasting Eq. (17) as:

$$T_\tau = \left(\frac{T_w - T_P}{K u_\tau + Pr_t U_P} \right) u_\tau \quad (21)$$

where K is a constant defined by the authors.³ In this way inserting Eq. (21) inside Eq. (20) provides a non-linear equation in u_τ . The wall-heat-flux for a given imposed temperature on the wall is finally given as:

$$q_w = \rho_w c_{p,w} u_\tau T_\tau \quad (22)$$

from which $\alpha_{t,w}$ can be defined from Eq. (16). Being a coupled model, this wall-function provides also the u_τ or equivalently the wall shear stress τ_w in output, thus not needing a closure model as that provided in Eq. (13).

Run	$\alpha_{t,w}$	u_τ	ε_P	$P_{k,P}$	k_P
RA-WF	Eq. (14)	Eq. (13)	Eq. (11)	Eq. (12)	Eq. (7)
TH-WF	Eq. (16)	Eq. (13)	Eq. (11)	Eq. (12)	Eq. (7)
C-WF	Eq. (16)	-	Eq. (11)	Eq. (12)	$\frac{\rho_w}{\rho_P} \frac{u_\tau^2}{C_\mu^{1/2}}$

Table 2: Summary of uRANS wall-modeled simulations of the single-injector GOx/GCH4 chamber.

4.2 Algebraic equilibrium wall-function for real-gas flows

Regarding the second case study examined in the present work a new algebraic wall-function is proposed, thought as an extension of the coupled model previously described³ to any arbitrary (real-gas) EoS and developed from a recently developed WR-LES database.¹¹ The proposed extension is based on a modification of step 3) outlined in Section 4.1 where the ideal-gas EoS came into play, and consists in:

- 3a) substituting $\rho/\rho_w = \mathcal{Z}_w T_w / \mathcal{Z} T$ in Eq. (18), with \mathcal{Z} the compressibility factor obtained from any arbitrary EoS (in the present work from NIST²⁷). After some re-arrangement we get:

$$\frac{(\mathcal{Z}_w T_w)^{1/2}}{Pr_\tau T_\tau} \int_{T_a}^{T_b} \left(\frac{1}{\mathcal{Z} T} \right)^{1/2} dT \approx \frac{1}{\kappa} \ln(y^+) + C \quad (23)$$

where Eq. (17) has been used to change the integration variable from dU^+ to dT and derive the integration bounds $T_a = T(U^+) = 0$ and $T_b = T(U^+ = 0)$. Based on the schematization of Fig. 2 we can observe that the integrand $L(T; p_0) = (1/\mathcal{Z} T)^{1/2}$ appearing in Eq. (23) is indeed a tabulated quantity, once p_0 which is the target thermodynamic pressure of the flow is set (5 MPa for the present analysis). An analytical fitting can therefore be obtained in a pre-processing step leading to a non-linear equation in u_τ similarly to Eq. (20) but now retaining variation of properties (density) in the boundary layer based on any arbitrary EoS. In the present work the proposed fitting is given by:

$$L(T; p_0) = \begin{cases} m \left(1 - \frac{1}{1 + e^{-n(T-T_0)}} \right) & T \leq T_0 \\ \frac{\delta}{(T + T^*)} & T > T_0 \end{cases} \quad (24)$$

and consists of a piece-wise sigmoid and hyperbolic functions. The functions parameters of Eq. (24) are determined by the user in pre-processing and for the present configuration are $m = 0.2793$, $n = 0.0539$, $\delta = 21.3112$ and $T^* = 92.3560$; $T_0 = 60.27$ K separates the low branches as displayed in Fig. 24.

5. Results

In this Section results of the applications on the configurations described in Section 2 are presented.

5.1 Case-study 1

Regarding uRANS simulations of the single-injector chamber, first a grid convergence analysis is led on 2D axis-symmetric domains in order to ensure the grid independence of the next results. To this end Fig. 3 displays wall-heat-fluxes ensuing from TH-WF described in Section 4 on a coarse, medium and fine wedge, respectively consisting of 224×26 , 548×52 and 1096×104 computational cells in the longitudinal-radial directions.

As no relevant differences are observed between the medium and fine resolution, the former is chosen as baseline mesh. This choice is further motivated by observing that with the coarse resolution substantial differences are observed right after the injection plane, outlining the importance of a refinement in that region. Results of the wall-function analysis are presented in Fig. 4. A summary of the performed simulations is reported in Tab. 2.

Wall-heat-flux predictions with different wall-function models for $\alpha_{t,w}$ described in Section 4.1 show how the progressively more detailed modelling of the thermal field results in a better reproduction of experimental data. In particular the coupled model provides the best agreement with the experiments, while both the thermal wall-function and RA-WF overestimate them (more drastically the latter than the former). This clearly indicates the importance of retaining the intrinsic coupling of thermal and kinematic fields for reliable wall-heat-flux predictions and the limits of the algebraic

VALIDATION AND DEVELOPMENT OF WALL-FUNCTIONS FOR LRE

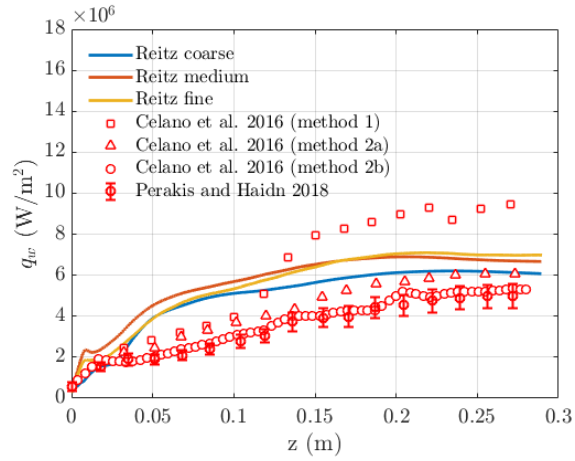


Figure 3: Grid convergence analysis on 2D meshes for TH-WF.

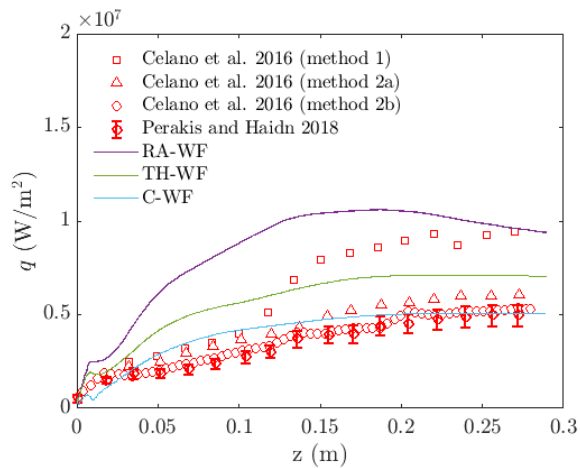


Figure 4: Analysis of wall-functions on 2D mesh of TUM single-injector.

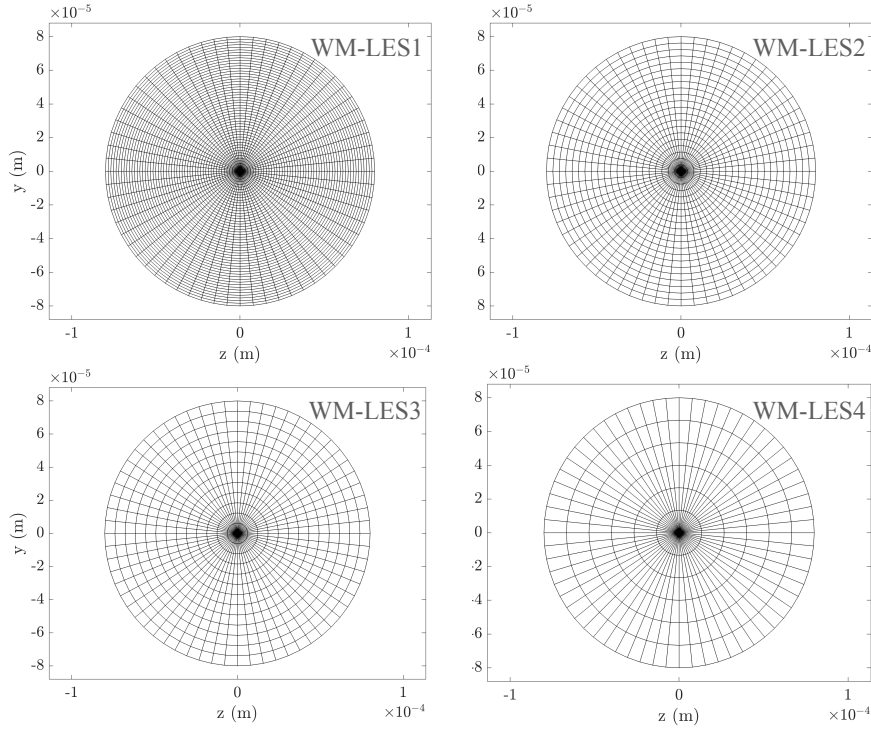


Figure 5: WM-LES grids for the a-priori application of wall-functions on the database.

closure of u_τ provided by Eq. (13), which is based on dimensional arguments and turbulence scalings mainly valid for incompressible flows. Poor agreement for C-WF is indeed found close to the injector region, that is around the first experimental points. There the equilibrium assumption, which stands at the ground of all the examined models, might indeed fails due to a recirculating flow region forming downstream the injection channel exit.

5.2 Case-study 2

In this Section an a-priori analysis of the wall-function proposed in Section 4.2 on the WR-LES database of Section 2 is reported. As a term of comparison, also the C-WF is tested, being the developed model thought as an extension of C-WF to any arbitrary EoS. It is worth reminding that here *a-priori* implies that values from the WR-LES simulations are used as input quantities for the selected wall-function models in order to reproduce WR-LES data for each case of Tab. 1.

The mentioned models are applied at selected sections along the pipe axis and on different wall-modeled grids (WM-LES) obtained by coarsening the wall-adjacent cell width of the original mesh and assuming an equispaced distribution in the radius. Figure 5 displays the so obtained WM-LES grids.

The a-priori analysis are displayed in Fig. 6 for the wall-function model C-WF and in Fig. 7 for the new model, both in terms of wall temperature and skin friction velocity compared to WR-LES corresponding data.

Results of the a-priori analysis show that the two models perform almost comparable for SP-Q1 on each simulated grid except for WM-LES1 due to the associated y^+ which is too low for wall-function applications ($y^+ \approx 10$ although not shown here); as the heat flux is increased however substantial deviations from the reference wall-resolved data are observed on both investigated models, with slight improvements of the newly developed model over the original C-WF. This outlines that, despite the ideal-gas EoS being a source of error for the original C-WF and the new proposed model providing an advancement in this sense, still another issue affects both the models and causes the observed trends. Among the derivation steps outlined in the previous section, the most critical one is indeed the assumption of validity of the Van Driest transformation.

The mentioned transformation is in fact based on dimensional arguments and aims at reproducing the correct slope in the log-layer assuming that the dominant effect of compressibility is mean property variation, most importantly density. Despite its accuracy being successfully tested on supersonic boundary layers over adiabatic walls both by means of DNS and experimental analysis, in the context of non-adiabatic conditions different authors^{8,15,17,22,28} outlined its inaccuracy, eventually proposing alternative velocity (U_I) and wall-distance (y_I) transformation paradigms expressed

VALIDATION AND DEVELOPMENT OF WALL-FUNCTIONS FOR LRE

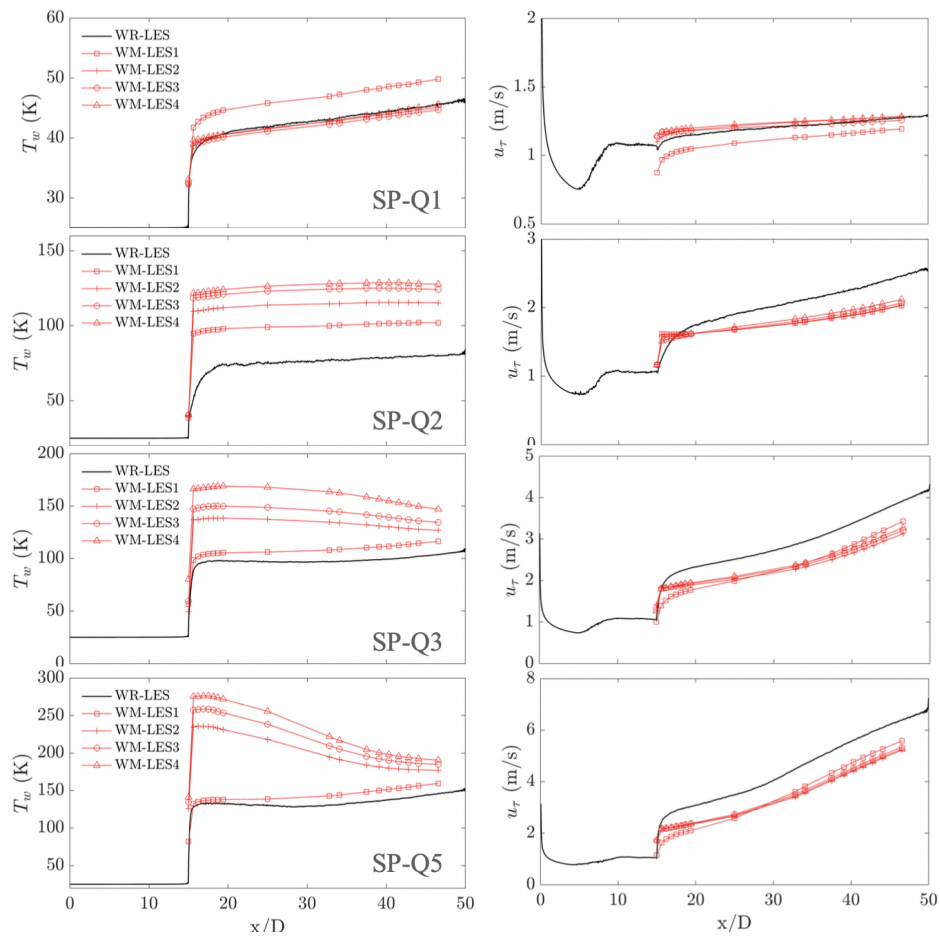


Figure 6: A-priori application of C-WF on the WR-LES database.

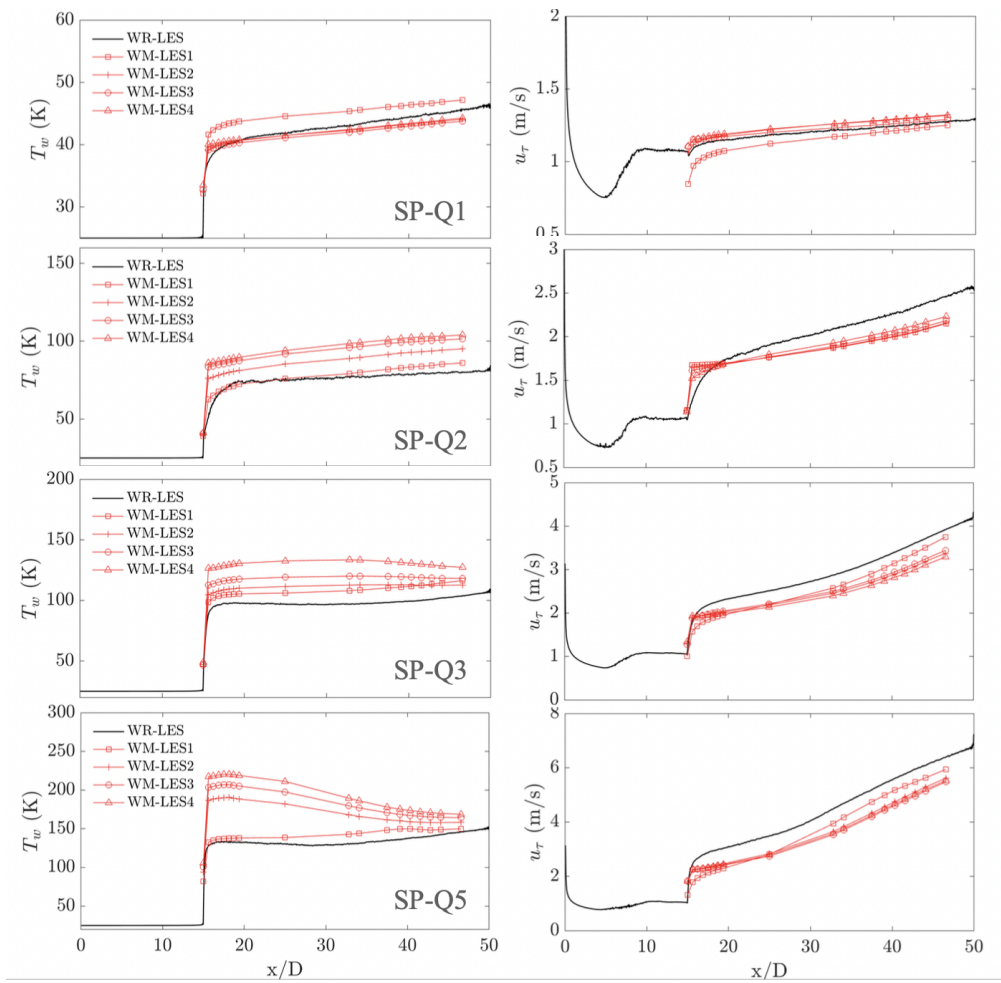


Figure 7: A-priori application of the real-gas extension of C-WF proposed in Section 4.2 on the WR-LES database.

VALIDATION AND DEVELOPMENT OF WALL-FUNCTIONS FOR LRE

Transformation	U^*	f	g
Van Driest ²⁹	U^+	$f_{VD} = 1$	$g_{VD} = \mathcal{D}^{1/2}$
Patel et al. ²²	U_{VD}^+	$f_P = \frac{d}{dy} \left(\frac{\mathcal{D}^{1/2} y}{\mathcal{V}} \right)$	$g_P = 1 + \frac{y\mathcal{V}}{Re_\tau \mathcal{D}^{1/2}} \frac{d}{dy} \left[Re_\tau \left(\frac{\mathcal{D}^{1/2}}{\mathcal{V}} \right) \right]$
Trettel et al. ²⁸	U^+	$f_T = \frac{d}{dy} \left(\frac{\mathcal{D}^{1/2} y}{\mathcal{V}} \right)$	$g_T = \mathcal{V} f_T$

Table 3: Summary of selected velocity transformations from literature: \mathcal{V} and \mathcal{D} are μ/μ_w and ρ/ρ_w respectively while $Re_\tau = yu_\tau/\nu_w$ is the friction Reynolds number.

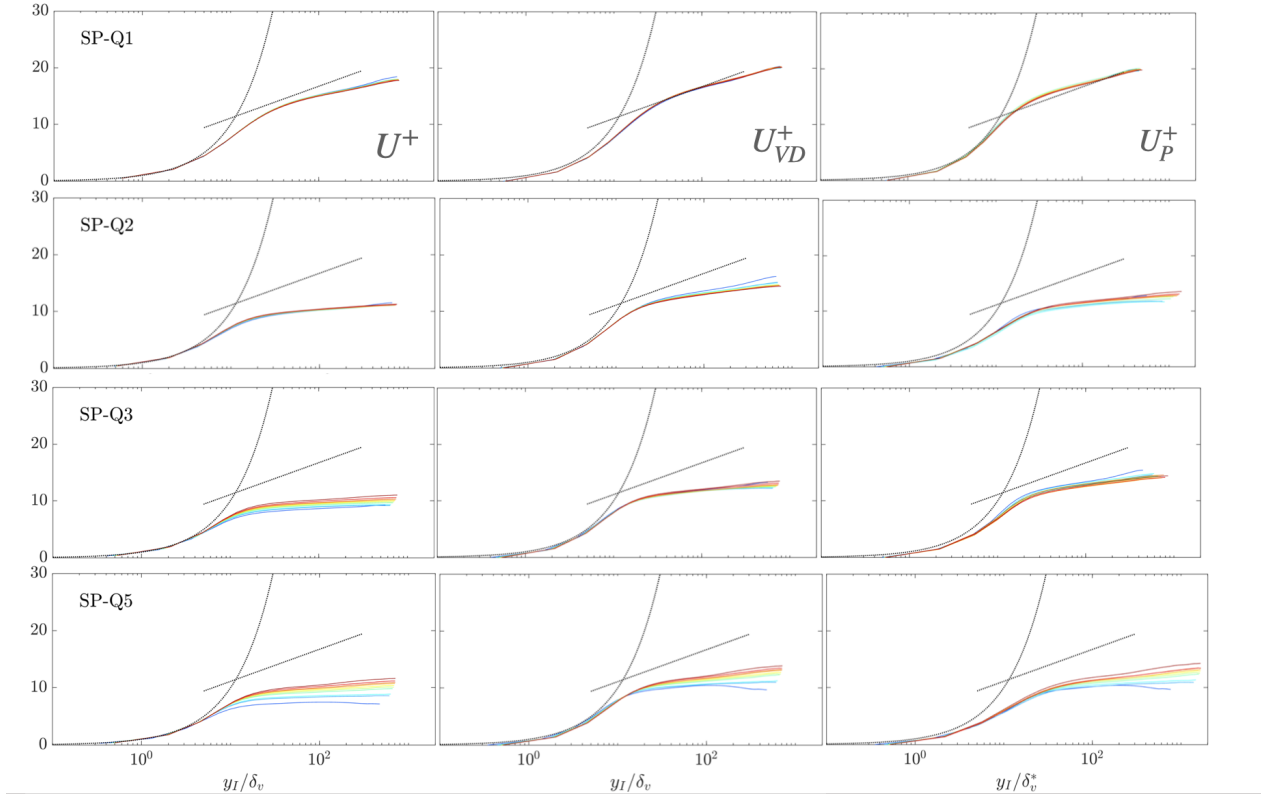


Figure 8: A-priori analysis of selected turbulent velocity scalings from Tab. 3 at different sections along the heated pipe segment. $\delta_v = \nu_w/u_\tau$ and $\delta_v^* = \nu/u_\tau^*$ with $u_\tau^* = \sqrt{\tau_w/\rho}$ are the standard and semi-local wall units, respectively.

as:¹⁷

$$y_I^+ = \int_0^y f dy \quad U_I^+ = \int_0^{U^*} g dU^* \quad (25)$$

Among the many, we mention here and compare the most employed summarized in Tab. 3.

Figure 8 displays the turbulent velocity transformations reported in Tab. 3 at different sections along the pipe length for each case of the database.

Results show that except for SP-Q1, for which all the selected transformations perform comparable in collapsing profiles at different sections and on the incompressible law of the wall, relevant deviations for each transformation (included the Van Driest's one) are observed for SP-Q2, SP-Q3 and SP-Q5. This seems to correlate with the results of Fig. 6 and Fig. 7, where increasing deviations from the wall-resolved results were observed on the mentioned cases.

6. Conclusions

In this work a wall-modeled framework has been proposed and applied to uRANS simulation of LRE combustion chambers. The proposed framework showed robust and efficient performances in predicting wall heat fluxes in LRE-relevant conditions, with an accuracy dependent on the employed wall-function model. Among the algebraic and equilibrium wall-models investigated, it was shown that retaining the intrinsic coupling of the kinematic and thermal

fields is a fundamental prerequisite in order to have reliable predictions of thermo-mechanical loads on the chamber wall, despite density-corrected closure model for the skin-friction velocity resulting in an improvement of non-coupled models.¹⁰ In the context of cryogenic, high pressure flows the application of algebraic wall-functions is still limited. In this context a-priori application on a recently proposed WR-LES database investigated the limits of these models, revealing that despite a thermodynamic-consistent extension of a coupled wall-model proposed by the authors to real-gas flows, the investigated model still presents some deviations while reproducing reference wall-resolved data. This seems to be associated to the Van Driest velocity transformation which is assumed to be valid for the considered supercritical cryogenic flow. An a-priori analysis on the mentioned and more sophisticated velocity transformations however showed how this is valid only under moderate stratification levels, that is for relatively low values of imposed heat flux. As the latter is increased all the considered transformations are shown to fail in collapsing velocity profiles at different sections of the pipe and on the incompressible law-of-the-wall.

7. Acknowledgments

The authors Italian Super Computing Center CINECA for the computational resources accessed through the ISCRA-C Project HP10CN0S3R. G. I. acknowledges the support of Lazio region in the context of "POR FESR LAZIO 2014-2020". The support of Sapienza University by means of the early stage researchers funding is also gratefully acknowledged.

References

- [1] C Angelberger, T Poinso, and B Delhay. Improving near-wall combustion and wall heat transfer modeling in si engine computations. Technical report, SAE Technical Paper, 1997.
- [2] Fabio Berni, Giuseppe Cicalese, and Stefano Fontanesi. A modified thermal wall function for the estimation of gas-to-wall heat fluxes in CFD in-cylinder simulations of high performance spark-ignition engines. *Applied Thermal Engineering*, 115:1045–1062, 2017.
- [3] Olivier Cabrit and Franck Nicoud. Direct simulations for wall modeling of multicomponent reacting compressible turbulent flows. *Physics of Fluids*, 21(5):055108, 2009.
- [4] TJ Craft, SE Gant, Hector Iacovides, and BE Launder. A new wall function strategy for complex turbulent flows. *Numerical Heat Transfer, Part B: Fundamentals*, 45(4):301–318, 2004.
- [5] TJ Craft, AV Gerasimov, H Iacovides, and BE Launder. Progress in the generalization of wall-function treatments. *International Journal of Heat and Fluid Flow*, 23(2):148–160, 2002.
- [6] Alberto Cuoci, Alessio Frassoldati, Tiziano Faravelli, and Eliseo Ranzi. Opensmoke++: An object-oriented framework for the numerical modeling of reactive systems with detailed kinetic mechanisms. *Computer Physics Communications*, 192:237–264, 2015.
- [7] Joel H Ferziger, Milovan Perić, and Robert L Street. *Computational methods for fluid dynamics*, volume 3. Springer, 2002.
- [8] Kevin Patrick Griffin, Lin Fu, and Parviz Moin. Velocity transformation for compressible wall-bounded turbulent flows with and without heat transfer. *Proceedings of the National Academy of Sciences*, 118(34), 2021.
- [9] Zhiyu Han and Rolf D Reitz. A temperature wall function formulation for variable-density turbulent flows with application to engine convective heat transfer modeling. *International journal of heat and mass transfer*, 40(3):613–625, 1997.
- [10] G Indelicato, PE Lapenna, A Remiddi, and F Creta. An efficient modeling framework for wall heat flux prediction in rocket combustion chambers using non adiabatic flamelets and wall-functions. *International Journal of Heat and Mass Transfer*, 169:120913, 2021.
- [11] Giuseppe Indelicato, Pasquale E Lapenna, Nelson P Longmire, Arianna Remiddi, Daniel T Banuti, and Francesco Creta. Dataset of wall-resolved large eddy simulations for the investigation of turbulent pseudo-boiling and wall-functions in cryogenic hydrogen pipe flows. In *AIAA SCITECH 2022 Forum*, page 0339, 2022.

VALIDATION AND DEVELOPMENT OF WALL-FUNCTIONS FOR LRE

- [12] Seong-Ku Kim, Miok Joh, Hwan Seok Choi, and Tae Seon Park. Multidisciplinary simulation of a regeneratively cooled thrust chamber of liquid rocket engine: Turbulent combustion and nozzle flow. *International Journal of Heat and Mass Transfer*, 70:1066–1077, 2014.
- [13] Nikolai Kornev and Egon Hassel. Method of random spots for generation of synthetic inhomogeneous turbulent fields with prescribed autocorrelation functions. *Communications in numerical methods in engineering*, 23(1):35–43, 2007.
- [14] Pasquale Eduardo Lapenna and Francesco Creta. Mixing under transcritical conditions: An a-priori study using direct numerical simulation. *The Journal of Supercritical Fluids*, 128:263–278, 2017.
- [15] Peter C. Ma, Xiang I. A. Yang, and Matthias Ihme. Structure of wall-bounded flows at transcritical conditions. *Phys. Rev. Fluids*, 3:034609, Mar 2018.
- [16] B Marracino and D Lentini. Radiation modelling in non-luminous nonpremixed turbulent flames. *Combustion science and technology*, 128(1-6):23–48, 1997.
- [17] Davide Modesti and Sergio Pirozzoli. Reynolds and mach number effects in compressible turbulent channel flow. *International Journal of Heat and Fluid Flow*, 59:33–49, 2016.
- [18] F. Moukalled, L. Mangani, and M. Darwish. *Turbulence Modeling*, pages 693–744. Springer International Publishing, Cham, 2016.
- [19] R. H. Nichols and C. C. Nelson. Wall function boundary conditions including heat transfer and compressibility. *AIAA Journal*, 42(6):1107–1114, 2004.
- [20] Franck Nicoud and Frédéric Ducros. Subgrid-scale stress modelling based on the square of the velocity gradient tensor. *Flow, turbulence and Combustion*, 62(3):183–200, 1999.
- [21] C. Maria Palma, S. Silvestri, G. Schlieben, C. Kirchberger, O. Haidn, and O. Knab. Injector characterization for a gaseous oxygen-methane single element combustion chamber. *Progress in Propulsion Physics*, 8:145–164, 2016.
- [22] Ashish Patel, Bendiks J Boersma, and Rene Pecnik. The influence of near-wall density and viscosity gradients on turbulence in channel flows. *Journal of Fluid Mechanics*, 809:793–820, 2016.
- [23] Nikolaos Perakis and Oskar J Haidn. Inverse heat transfer method applied to capacitively cooled rocket thrust chambers. *International Journal of Heat and Mass Transfer*, 131:150–166, 2019.
- [24] Norbert Peters. Laminar diffusion flamelet models in non-premixed turbulent combustion. *Progress in energy and combustion science*, 10(3):319–339, 1984.
- [25] C.D. Rakopoulos, George Kosmadakis, and Efthimios Pariotis. Critical evaluation of current heat transfer models used in CFD in-cylinder engine simulations and establishment of a comprehensive wall-function formulation. *Applied Energy*, 87:1612–1630, 05 2010.
- [26] Rolf D. Reitz. Assessment of wall heat transfer models for premixed-charge engine combustion computations. In *International Congress & Exposition*. SAE International, feb 1991.
- [27] Vincent K Shen, DW Siderius, WP Krekelberg, HW Hatch, et al. Nist standard reference simulation website. *NIST standard reference database*, (173):20899, 2017.
- [28] Andrew Trettel and Johan Larsson. Mean velocity scaling for compressible wall turbulence with heat transfer. *Physics of Fluids*, 28(2):026102, 2016.
- [29] E. R. Van Driest. Turbulent boundary layer in compressible fluids. *Journal of the Aeronautical Sciences*, 18(3):145–160, 1951.
- [30] Henry G Weller, Gavin Tabor, Hrvoje Jasak, and Christer Fureby. A tensorial approach to computational continuum mechanics using object-oriented techniques. *Computers in physics*, 12(6):620–631, 1998.